Earthquake Engineering & Structural Dynamics
The Journal of the International Association for Earthquake Engineering

EARTHQUAKE ENGINEERING & STRUCTURAL DYNAMICS
Earthquake Engng Struct. Dyn. (2015)
Published online in Wiley Online Library (wileyonlinelibrary.com). DOI: 10.1002/eqe.2608

An analytical model of a deformable cantilever structure rocking on a rigid surface: development and verification

Michalis F. Vassiliou*,†, Rico Truniger and Božidar Stojadinović

Institute of Structural Engineering (IBK), Swiss Federal Institute of Technology (ETHZ), Wolfgang-Pauli-Strasse 15, 8093 Zürich, Switzerland

SUMMARY

This paper extends previously developed models to account for the influence of the column and the foundation masses on the behavior of top-heavy deformable elastic cantilever columns rocking on a rigid support surface. Several models for energy dissipation at impact are examined and compared. A novel Vertical Velocity Energy Loss model is introduced. Rocking uplift and overturning spectra for the deformable elastic cantilever model excited by sinusoidal ground motions are constructed. The effects of non-dimensional model parameter variations on the rocking spectra and the overturning stability of the model are presented. It is shown that the remarkable overturning stability of dynamically excited large cantilever columns is not jeopardized by their deformability. Copyright © 2015 John Wiley & Sons, Ltd.

Received 24 October 2014; Revised 26 March 2015; Accepted 26 June 2015

KEY WORDS: seismic isolation; rocking; earthquake engineering; uplifting structures; wind turbines; overturning

1. INTRODUCTION

The response of rigid blocks allowed to uplift and rock on a rigid foundation under seismic ground motion excitation has been studied for more than a century (Milne [1]). Housner [2] demonstrated a size effect that characterizes the rocking response of rigid blocks subjected to a ground motion excitation: (i) larger objects need a larger ground acceleration to overturn, and (ii) earthquakes with longer dominant periods have a larger overturning capability than those shorter dominant periods. The fundamental reason for this size effect is the inertia term in the equation of motion of a rigid block that is proportional to the 4^{th} power of the linear dimension characterizing the size of the block, while all other terms are proportional to the 3^{rd} power of the block size. The above results were presented in the form of rocking spectra for pulse-like ground motion records by Zhang and Makris [3] and Makris and Konstantinidis [4]. Makris and Vassiliou [5, 6] have studied rigid blocks assemblies and have concluded that a class of top-heavy rocking block assemblies is, counter-intuitively, stable. This explains the survival of ancient Greek and Roman top-heavy temple structures in regions of high seismicity despite the lack of historical evidence that ancient engineers were aware of the size effect in rocking.

This size effect has led researchers to propose free rocking as a seismic response modification technique. Structures designed to uplift at the base and rock are characterized by small residual displacements and small forces transmitted to foundations (Apostolou *et al.* [7], Gelagoti *et al.* [8], Makris and Vassiliou [5], Antonellis and Panagiotou [9], Makris [10, 11]). It should be stated that the concept of free rocking is different from the concept of controlled rocking of post-tensioned

*Correspondence to: Michalis F. Vassiliou, Institute of Structural Engineering (IBK), Swiss Federal Institute of Technology (ETHZ), Wolfgang-Pauli-Strasse 15, 8093 Zürich, Switzerland.
†E-mail: mfvassiliou@gmail.com

moment resisting frame and shear wall systems described in [12–19] and references therein. Controlled rocking structures uplift and rock, but utilize post-tensioning cables and special-purpose energy dissipation elements installed at the rocking connections to reduce lateral displacements.

Large structures, such as tall chimneys and tall bridges, are ideal candidates for rocking seismic response modification because of the size effect. A 60-m tall bridge that uses rocking in such manner has already been built across the Rangitikei River in New Zealand in 1981 [20, 21]. Moreover, a 33-m tall chimney at the Christchurch New Zealand airport has been designed to uplift (Sharpe and Skinner [22]). Furthermore, three 30-m to 38-m tall chimneys in Piraeus, Greece, have been retrofitted taking into account their rocking behavior [23].

Large slender structures are, however, deformable: they deform to the extent that the rigid body assumption cannot be justified. To this end, several models for rocking of deformable bodies have been proposed by Psycharis [24], Oliveto *et al*. [25], Apostolou *et al*. [7], Ma [26], Chopra and Yim [27] and Vassiliou *et al*. [28]. Recently, Acikgoz and DeJong [29] refined Olivetto *et al*.'s [25] model (a massless elastic column with a concentrated mass at the top on a rigid massless base) and studied the behavior of this model using dimensional analysis. They concluded that structural deformability modifies the response of rocking structures, but that it does not jeopardize their dynamic stability.

Modeling rocking response of elastic structures whose mass is distributed along their height as well as structures with foundations whose mass cannot be neglected, requires an extension of the Oliveto *et al*. [25] model to include the mass of the column and the mass of the foundation (Figure 1). A model for uplifting and rocking of such structures on a rigid support surface excited by horizontal ground motion excitation is developed herein. Verification and validation of this model are presented in the companion paper [30]. The observations stemming from this model are compared to the findings of Acikgoz and DeJong [29]. Housner-like coefficients of restitution are derived, assuming conservation of angular momentum as was done in [10, 31]. Rocking spectra are constructed and the influence of deformability on the overturning stability of the model is investigated. Possible candidates for rocking response modification strategies that are qualitatively well described by a rocking top-heavy deformable cantilever structure are wind turbines. Therefore, rocking spectra are constructed for non-dimensional parameter values that correspond to wind turbine structures.

2. PROPOSED ROCKING MODEL

2.1. Equations of motion

A deformable rocking column with a uniformly distributed stiffness EI and mass, and a concentrated mass on the top supported by a rigid massive base is shown in Figure 1. The column mass is uniformly distributed along its length, totaling m_c. The concentrated mass m on the top that has no moment of inertia. The base has a mass m_b and a moment of inertia around its center of its mass I_b.

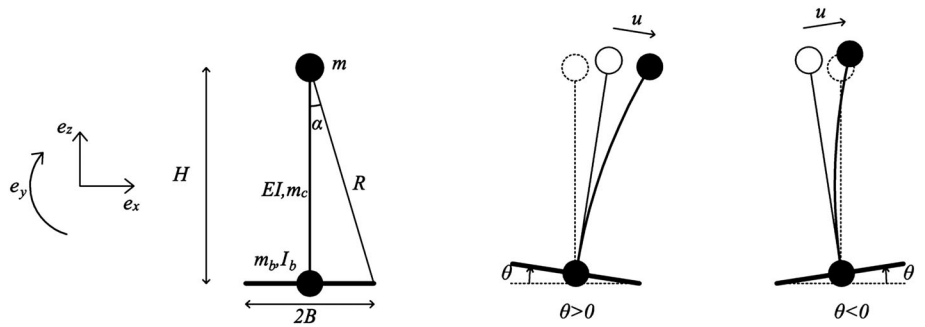

Figure 1. Deformable rocking structure with two lumped masses at the top and the base, and a column with a uniformly distributed mass.

DOI: 10.1002/eqe

The thickness of the base is negligible compared to the height, H, of the column. The width of the base is $2B$. The slenderness, α, of the system is defined as $\alpha = \text{atan}(B/H)$. The base rotation is defined as θ, and the horizontal displacement of the top of the column with respect to the bottom of the column is defined as u (see Figure 1). The column and the foundation are rigidly connected such that uplifting and rocking occur as shown in Figure 1. The rocking surface is assumed to be rigid. This assumption is adequate to describe the small-scale models studied in the companion paper [30]. For real structures, such as tall bridge columns, chimneys or wind turbines, rocking on the ground (or on a rigid foundation that rests on the ground) this assumption might lead to unrealistically intense impacts which may, in turn, lead to more intense high frequency elastic vibration. Rocking on deformable ground lies beyond the scope of this paper.

The column is treated as a continuous dynamic system with the following deformation shape function:

$$\psi(\xi) = \frac{3\xi^2}{2H^2} - \frac{\xi^3}{2H^3} \tag{1}$$

where ξ is the absolute distance measured from the base of the column. Because the system has distributed mass, the shape function (1) is an approximation that gives relatively accurate results for fixed base systems [32]. Hence, the deformation of the column is given by:

$$u_\xi(\xi, t) = u(t)\psi(\xi). \tag{2}$$

When there is no uplift, the motion of the system is described using only one degree of freedom, the relative displacement of the top of the column, u. The equation of motion of the column is:

$$\ddot{u} + 2\zeta\omega_n\dot{u} + {\omega_n}^2 u = -\widetilde{\Gamma}\ddot{u}_g \tag{3}$$

where:

$$\omega_n = \frac{\widetilde{k}}{\widetilde{m}}, \tag{4}$$

$$\widetilde{k} = \int_0^H EI\left(\psi''(\xi)\right)^2 d\xi = \frac{3EI}{H^3}, \tag{5}$$

$$\widetilde{m} = \int_{column} (\psi(\xi))^2 dm + m = m + \frac{33}{140}m_c, \tag{6}$$

$$\widetilde{\Gamma} = \frac{m + \int_{column} \psi(\xi) dm}{m + \int_{column} (\psi(\xi))^2 dm} = \frac{m + \frac{3}{8}m_c}{m + \frac{33}{140}m_c}. \tag{7}$$

In equation (3), ζ is the damping ratio associated with energy dissipated in the column while it vibrates, but not with the energy dissipation at the rocking interface. This damping is assumed to be viscous and classical.

Two degrees of freedom, the base rotation θ and the relative displacement of the column u, are used to describe the motion of the model when the base uplifts. Using a Lagrangian formulation (see Appendix) the following equations of motions are obtained:

DOI: 10.1002/eqe

$$\left(I_{bc}+m_c\left(B^2+\frac{H^2}{3}\right)+\frac{33}{140}m_cu^2-sign(\theta)\frac{3}{4}Bum_c+m\left(B^2+H^2\right)-sign(\theta)2Bum+mu^2\right)\ddot{\theta}=$$
$$=-\left(\frac{33}{70}m_c+2m\right)u\dot{u}\dot{\theta}-\left(\frac{11}{40}m_c+m\right)H\ddot{u}+sign\ \theta\left(\frac{3}{4}m_c+2m\right)B\dot{u}\dot{\theta}+$$
$$+\ddot{u}_g\left(-sign(\theta)(m+m_c+m_b)B\sin\theta-\left(\frac{m_c}{2}+m\right)Hcos\ \theta+\left(\frac{3}{8}m_c+m\right)u\sin\theta\right)$$
$$+g\left(-sign(\theta)(m+m_c+m_b)B\cos\theta+\left(\frac{m_c}{2}+m\right)H\sin\theta+\left(\frac{3}{8}m_c+m\right)u\cos\theta\right), \tag{8}$$

$$\left(\frac{33}{140}m_c+m\right)\ddot{u}+\left(\frac{11}{40}m_c+m\right)H\ddot{\theta}=-\frac{3EI}{H^3}u-c\dot{u}+\left(\frac{3}{8}m_c+m\right)g\sin\theta+$$
$$+\left(\left(\frac{33}{140}m_c+m\right)u-sign(\theta)\left(\frac{3}{8}m_c+m\right)B\right)\dot{\theta}^2-\left(\frac{3}{8}m_c+m\right)\ddot{u}_g\cos\theta \tag{9}$$

where I_{bc} is the moment of inertia of the base around the pivot point. Equation (8) expresses moment equilibrium around the pivot point, and equation (9) expresses force equilibrium in the direction of deformation u in the deformed configuration.

2.2. *Modal analysis*

It has been shown [27, 29] that an uplifted column has a larger eigenfrequency compared to the same column before uplifting. To compute this frequency, equations (8) and (9) are linearized, and the gravity and forcing terms are neglected. Equation (8) gives:

$$\left[I_{bc}+m_c\left(B^2+\frac{H^2}{3}\right)+m\left(B^2+H^2\right)\right]\ddot{\theta}+\left(\frac{11}{40}m_c+m\right)H\ddot{u}=0. \tag{10}$$

Equation (9) gives:

$$\left(\frac{33}{140}m_c+m\right)\ddot{u}+\left(\frac{11}{40}m_c+m\right)H\ddot{\theta}+c\dot{u}+\frac{3EI}{H^3}u=0. \tag{11}$$

Equations (10) and (11) can be written in matrix form:

$$\mathbf{M}\ddot{\mathbf{U}}+\mathbf{C}\dot{\mathbf{U}}+\mathbf{K}\mathbf{U}=\mathbf{0} \tag{12}$$

where:

$$\mathbf{M}=\begin{bmatrix}\left(\frac{33}{140}m_c+m\right) & \left(\frac{11}{40}m_c+m\right)H\\ \left(\frac{11}{40}m_c+m\right)H & I_{bc}+m_c\left(B^2+\frac{H^2}{3}\right)+m\left(B^2+H^2\right)\end{bmatrix}, \tag{13}$$

$$\mathbf{C}=\begin{bmatrix}c & 0\\ 0 & 0\end{bmatrix}, \tag{14}$$

DOI: 10.1002/eqe

$$\mathbf{K} = \begin{bmatrix} \dfrac{3EI}{H^3} & 0 \\ 0 & 0 \end{bmatrix}, \tag{15}$$

$$\mathbf{U} = \begin{bmatrix} u \\ \theta \end{bmatrix}. \tag{16}$$

The eigenfrequency equation:

$$\left|\mathbf{K} - {\omega_{up}}^2 \mathbf{M}\right| = 0 \tag{17}$$

gives:

$$\omega_{up,1} = 0 \quad \text{and} \quad \omega_{up,2} = \omega_n \sqrt{\frac{I_{bc} + m_c\left(\frac{H^2}{3} + B^2\right) + m\left(H^2 + B^2\right)}{I_{bc} + m_c\left(\frac{H^2}{3} + B^2\right) + m\left(H^2 + B^2\right) - \frac{\left(m + \frac{11}{40}m_c\right)^2 H^2}{m + \frac{33}{140}m_c}}}. \tag{18}$$

Because the uplifted structure is a mechanism, the first eigenmode represents rigid body motion around the pivot point. The damping ratio of the second eignemode (that involves deformation of the column) is:

$$\zeta_{up} = \zeta \sqrt{\frac{I_{bc} + m_c\left(\frac{H^2}{3} + B^2\right) + m\left(H^2 + B^2\right)}{I_{bc} + m_c\left(\frac{H^2}{3} + B^2\right) + m\left(H^2 + B^2\right) - \frac{\left(m + \frac{11}{40}m_c\right)^2 H^2}{m + \frac{33}{140}m_c}}}. \tag{19}$$

For a massless column and a massless base the above equations give:

$$\omega_{up,2} = \omega_n \frac{R}{B} \quad \textit{and} \quad \zeta_{up,2} = \zeta \frac{R}{B}. \tag{20}$$

These values were first obtained by Chopra and Yim [27].

Equations (18) and (19) show that the fundamental vibration frequency and the damping ratio of the uplifted column are larger than those of the corresponding fixed-base column. The difference is the largest for massless base and column. In the limit case of a very large base, where $I_{bc} \to \infty$, the fundamental vibration frequency and the damping ratio of the uplifted column tend to those of the fixed-base column.

2.3. Uplift

The overturning (ot) and the restoring (rt) moments of the column in Figure 1, taken about the pivot corner point, are, respectively:

$$M_{ot} = -\left(m\ddot{u}^{total}H + \int\limits_{column} \ddot{u}^{total}\psi(\xi)\xi dm\right) = -\ddot{u}H\left(m + \frac{11}{40}m_c\right) - \left(m + \frac{m_c}{2}\right)\ddot{u}_g H, \tag{21}$$

DOI: 10.1002/eqe

$$M_{rt} = (m_b + m_c + m)gB \mp \left(\frac{3}{8}m_c + m\right)gu \tag{22}$$

where the upper and the lower signs denote moments about the right and the left pivot corner point, respectively. Hence, the condition for uplift is:

$$\pm(M_{ot} + M_{rt}) > 0. \tag{23}$$

Equations (3) and (21–23) define the uplift condition:

$$\pm H\left(m + \frac{11}{40}m_c\right)\left({\omega_1}^2 u + 2\zeta\omega_1\dot{u} + \widetilde{\Gamma}\ddot{u}_g\right) \mp \left(m + \frac{m_c}{2}\right)\ddot{u}_g H - (m_b + m_c + m)Bg \pm \left(\frac{3}{8}m_c + m\right)ug > 0. \tag{24}$$

For undamped systems with $u << B$ and $m_c << m$ the above equation can be simplified to [29]:

$$|u| > \frac{m_b + m}{m}\frac{Bg}{H{\omega_n}^2}. \tag{25}$$

This is the simplified uplift condition for the system in Figure 1.

2.4. Impact

Because Housner published his seminal paper [2] in 1963, numerous researchers working on rocking of rigid structures used the coefficient of restitution defined therein. This coefficient is based on the assumptions that the impact is instantaneous and that all of the impact forces are concentrated at the impacting corner point. This approach enabled Housner to use the conservation of angular momentum theorem (taken about the impacting corner) to compute the restitution coefficient. Accordingly, the energy lost in every impact is a function of the geometry of the rocking body alone, and it does not depend on the impact velocity or on the mechanical properties of the impacting surfaces. Intuition and experiments [21, 26, 33, 34] suggest that this does not hold. This has led researchers to consider the coefficient of restitution as an independent parameter of the problem [35, 36], or to use different impact models [37, 38].

Olieveto *et al*. [23] claimed that Chopra and Yim [27] and Psycharis [39] models, when applied to stiff rocking structures, develop inexplicably large elastic deformations. This has led to the development of new models. Olivetto [25] and Acikgoz and DeJong [29] models (both considering a massless deformable column on a massless rigid base with a lumped mass on the top) force the column base at incipient impact (Figure 2) to either stick on the ground and experience a full contact phase, or to immediately uplift about the opposite corner and continue to rock. The choice between these two possible states is made by considering the minimum of the total energy of the rocking system in conjunction with the constraint that the post-impact kinetic energy must be less than the pre-impact kinetic energy. This approach is an extension of Housner's approach. The latter constraint is enforced because the application of conservation of angular momentum on deformable rocking columns (as opposed to rigid rocking bodies) leads, in certain cases, to energy increase after impact. The conditions when such inconsistency occurs and graphical proofs that the energy increases are shown in Figure 2. In these cases, Acikgoz and DeJong enforced energy decrease by changing the conservation principle used [29, 40] from the Hounser-like conservation of the angular momentum to conservation of the horizontal momentum.

Even though another rocking state transition approach will be used in this paper, the Acikgoz and DeJong approach for modeling energy dissipated at impact is extended (ADJex) to the deformable rocking column model in Figure 1 for completeness and to allow for experimental validation in the companion paper [30]. Conservation of the angular momentum around the impacting corner gives

DOI: 10.1002/eqe

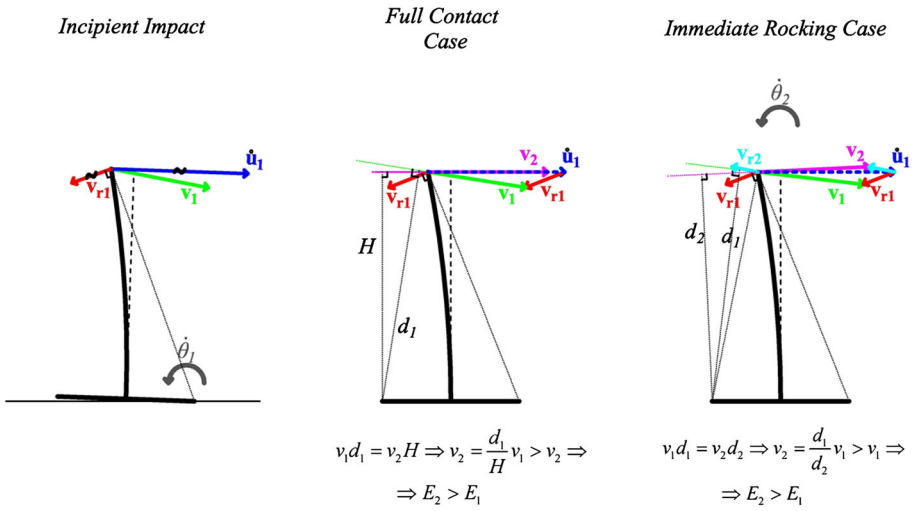

Figure 2. Let vector v_{r1} denote the velocity of the top of the column because of rotation velocity $\dot{\theta}_1$ and vector v_1 denote the total velocity of the top of the column before impact. Let $\dot{u}_1$ denote the pre- and post-impact horizontal velocity of the top of the column, assumed to remain the same before and after impact in the Acikgoz and DeJong approach [29]. In the Full Contact phase, v_2 is the total post-impact velocity vector. In the Immediate Rocking phase v_{r2} is the post-impact velocity component because of rotation $\dot{\theta}_2$ and v_2 is the total post-impact velocity vector. Conservation of angular momentum and the geometric relation between vectors v_1 and v_2 indicate that the post-impact energy of the system, E_2, is larger than the pre-impact energy of the system, E_1.

two expressions for the kinetic energy of the system, one for the full contact phase and the other for the immediate rocking phase. Note that the potential energy of the system does not change, because the system does not change position during the impact; thus, the kinetic energy expressions are sufficient to describe the change in the total energy of the system. In the full contact phase:

$$\dot{u}_2 = \frac{\left(I_{bc} - 2m_b B^2 + m_c\left(-B^2 + \frac{H^2}{3} + \frac{33}{140}u^2\right) + m\left(-B^2 + H^2 + u^2\right)\right)}{\left(\frac{11}{40}m_c + m\right)H}\dot{\theta}_1 + \dot{u}_1 \tag{26}$$

for impact on either the right or the left corner. The indices '1' and '2' denote the pre- and the post-impact states of the system in Figure 1. The kinetic energy in the full contact phase is:

$$E_{2,fc} = \frac{1}{2}\left(m + \frac{33}{140}m_c\right)\dot{u}_2{}^2 \tag{27}$$

with $\theta_2 = \dot{\theta}_2 = 0$ and, because the impact is instantaneous, $u_2 = u_1$.

In the immediate rocking phase there are two unknown quantities, the post-impact angular velocity of the base, $\dot{\theta}_2$ and the post-impact relative horizontal velocity of the top mass with respect to the bottom of the column, $\dot{u}_2$. Hence, an additional equation is needed. Acikgoz and DeJong [29] assumed that the relative horizontal velocity remains the same after impact (i.e. $\dot{u}_2 = \dot{u}_1$). Adopting this assumption and applying conservation of angular momentum around the impacting corner [40] gives:

$$\dot{\theta}_2 = \frac{\left(I_{bc} - 2B^2 m_b\right) + m_c\left(-B^2 + \frac{H^2}{3} + \frac{33}{140}u_1{}^2\right) + m\left(-B^2 + H^2 + u_1{}^2\right)}{I_{bc} + m_c\left(B^2 + \frac{H^2}{3} + \frac{33}{140}u_1{}^2 \pm \frac{3}{4}Bu_1\right) + m\left(B^2 + H^2 + u_1{}^2 \pm 2Bu_1\right)}\dot{\theta}_1 \tag{28}$$

where the upper sign corresponds to impact on the left corner and the lower to impact on the right corner. The kinetic energy of the immediate rocking phase is:

DOI: 10.1002/eqe

$$E_{2,r} = \frac{1}{2} I_{bc} \dot{\theta}^2 + \frac{1}{2} m_c \left(\left(B^2 + \frac{H^2}{3} + \frac{33}{140} u^2 \pm \frac{3}{4} Bu \right) \dot{\theta}_2{}^2 + \frac{33}{140} \dot{u}_2{}^2 + \frac{11}{20} H \dot{\theta}_2 \dot{u}_2 \right) + \\ + \frac{1}{2} m \left(\left(B^2 + H^2 + u^2 \pm 2Bu \right) \dot{\theta}_2{}^2 + \dot{u}_2{}^2 + 2H \dot{\theta}_2 \dot{u}_2 \right) \tag{29}$$

with the sign convention adopted for equation (22).

Let E_1 be the prior-to-the-impact energy of the system in Figure 1. In the case when $\min(E_r, E_{fc}) > E_1$ (which is possible, as shown in Figure 2), conservation of horizontal momentum is applied to yield:

$$\dot{u}_2 = \frac{\left(\frac{m_c}{2} + m \right) H}{\frac{3}{8} m_c + m} \dot{\theta}_1 + \dot{u}_1. \tag{30}$$

The ADJex model for energy dissipation at impact has the following shortcomings: (i) the choice of model state based on minimum energy is not theoretically consistent; (ii) because, in certain cases, the energy loss does not emerge naturally, it has to be enforced; and (iii) the 'double impact' mode of the ADJex model was not observed in experiments presented in the companion paper [30].

Therefore, a modification of Chopra and Yim [27] model, the Vertical Velocity Energy Loss (VVEL) model for energy dissipation at impact, is proposed, and equations that describe the rocking motion of the model shown in Figure 1 are derived. The VVEL model is based on the assumption that the kinetic energy associated with the vertical components of the velocities of the model in Figure 1 is lost at impact. The kinetic energy involving the horizontal component of the pre-impact velocity is given by:

$$E_{1,vh} = \frac{1}{2} m \left(H \dot{\theta}_1 + \dot{u}_1 \right)^2 + \frac{1}{2} m_c \left(\frac{H^2}{3} \dot{\theta}_1{}^2 + \frac{11}{20} H \dot{\theta}_1 \dot{u}_1 + \frac{33}{140} \dot{u}_1{}^2 \right). \tag{31}$$

Equating equations (27) and (31), the post-impact elastic velocity becomes:

$$\dot{u}_2 = sign\left(H \dot{\theta}_1 + \dot{u}_1 \right) \sqrt{\frac{m \left(H \dot{\theta}_1 + \dot{u}_1 \right)^2 + m_c \left(\frac{H^2}{3} \dot{\theta}_1{}^2 + \frac{11}{20} H \dot{\theta}_1 \dot{u}_1 + \frac{33}{140} \dot{u}_1{}^2 \right)}{m + \frac{33}{140} m_c}}. \tag{32}$$

For rigid models, the above equations gives $E_2/E_1 = \cos\alpha$, while Housner's approach gives $E_2/E_1 = \cos 2\alpha$. Hence, the proposed VVEL model dissipates less energy than the Housner model.

The response obtained by the proposed VVEL model is compared to that obtained using the ADJex model for the system in Figure 1 subjected to the same one-cycle sinusoidal pulse horizontal support acceleration used by Acikgoz and DeJong [29]. The responses of the two models are compared in Figures 3 and 4. Quantities α, the slenderness of the rocking system, u_{cr}, the relative displacement of the elastic column when uplift occurs, E_{ref}, the reference energy, and τ, the normalized time, are defined in the next section. The response of the models, in terms of the rotation angle, relative horizontal displacement of the top of the column and the kinetic energy of the system are compared in Figure 3 for the first three rocking impacts. Figure 4 shows zoomed-in views of the rotation angle and the kinetic energy graphs at the first (at about 0.9 s) and the second impact (at about 2.5 s). The VVEL model dissipates less energy than the ADJex model, as it is clearly seen in Figure 3. The 'double impact' mode occurs in the ADJex model as shown in Figure 4. The VVEL model for energy dissipation at impact is chosen for further study, even though it is noted that it might overestimate the elastic part of the rocking response of stiff deformable columns. Such cases point to the need to further refine the model for energy dissipation at impact.

DOI: 10.1002/eqe

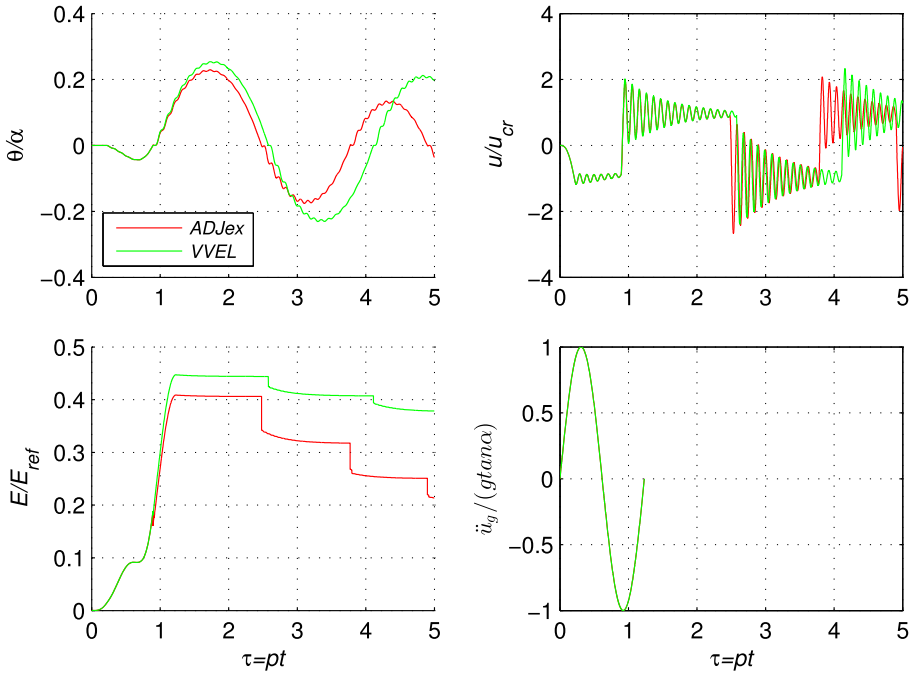

Figure 3. Rotation (top left), relative horizontal displacement (top right) and kinetic energy (bottom left) response of the model in Figure 1 when subjected to a one cycle sinusoidal pulse excitation (bottom right) for $A/(g\tan\alpha)=1.30$, $\omega_n/p=11.9$, $\omega/p=5.1$, $\alpha=0.2$ and $\zeta=0.005$.

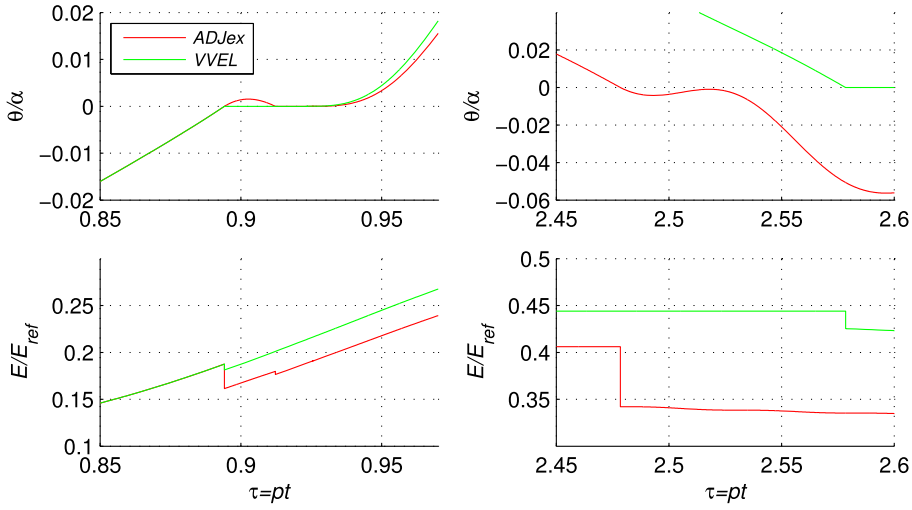

Figure 4. Zoomed-in views of the first two impacts at 0.9 s and 2.5 s in Figure 3.

3. DIMENSIONAL ANALYSIS OF THE ROCKING DEFORMABLE CANTILEVER

Physically realizable ground motion pulses can adequately describe the impulsive character of near-fault ground motions both qualitatively and quantitatively. Two parameters are needed to describe such pulses. These parameters are either the acceleration amplitude, a_p, and dominant cyclic frequency, ω_p, or the velocity amplitude, v_p, and dominant cyclic frequency, ω_p of the pulse [41, 42]. The response of the model in Figure 1 with VVEL energy dissipation model to an idealized acceleration pulse characterized by its amplitude, a_p, and dominant cyclic frequency, ω_p, [43] is examined. The response is a function of 12 variables:

DOI: 10.1002/eqe

$$(u,\theta) = f\left(EI, m, m_c, m_b, I_b, \zeta, \alpha, R_o, g, \omega_p, a_p, t\right) \tag{33}$$

involving three fundamental dimensions. According to Buckingham's Π-theorem [44] the response can be described by 12-3 = 9 dimensionless parameters:

$$\left(\frac{u}{u_{cr}}, \frac{\theta}{\theta_{cr}}\right) = \varphi\left(\frac{\omega_n}{p}, \frac{\omega_p}{p}, \gamma_{m_c}, \gamma_{m_b}, \gamma_{I_b}, \zeta, \alpha, \frac{a_p}{g\tan\alpha}, \tau\right) \tag{34}$$

where

$$\omega_n = \sqrt{\frac{\frac{3EI}{H^3}}{\left(m + \frac{33}{140}m_c\right)}}, \tag{35}$$

$$p = \sqrt{\frac{g}{R}}, \tag{36}$$

$$\gamma_{m_c} = \frac{m_c}{m}, \quad \gamma_{m_b} = \frac{m_b}{m}, \quad \gamma_{I_b} = \left(\frac{I_{bc}}{\frac{4}{3}m_b B^2}\right), \tag{37}$$

$$\tau = pt. \tag{38}$$

A critical rotation angle of the rigid rocking block is defined as the angle of unstable equilibrium:

$$\theta_{cr} = \tan^{-1}\left(\frac{m + m_b + m_c}{m + \frac{m_c}{2}}\frac{B}{H}\right). \tag{39}$$

A critical displacement u_{cr} is defined as the elastic displacement of the column when base statically uplifts:

$$u_{cr} = \frac{(m + m_b + m_c)Bg}{\left(m + \frac{11}{40}m_c\right)H\omega_n{}^2 + \left(\frac{3}{8}m_c + m\right)g}. \tag{40}$$

Following Acikgoz and DeJong, the total energy of the system is normalized by E_{ref}, which is defined as the difference in the potential energy of the rigid, top-heavy rocking column between the position of unstable equilibrium and the at-rest position.

3.1. Range of interest of dimensionless parameters

The range of values of the dimensionless parameters for a model in Figure 1 that corresponds to a wind turbine prototype structure is examined below.

- Dimensionless structural frequency: $\frac{\omega_n}{p}$

Prowel and Veels [45] state that the empirical relations between height and fundamental vibration period for buildings are not appropriate for wind turbines. They propose the relation:

$$T_n = 0.015h^{1.183} \tag{41}$$

where T_n is given in seconds and h in meters. Assuming $h \approx R$ the above equation gives:

$$\frac{\omega_n}{p} = \frac{133.7}{h^{0.683}} \tag{42}$$

DOI: 10.1002/eqe

where h is in meters. The tallest massively produced wind turbine is about 140 m tall [46], giving $\omega_n/p = 4.57$. Given the need for even taller wind turbines a lower bound of $\omega_n/p = 2.5$, corresponding to a height of 340 m is chosen.

- Dimensionless structural size: $\frac{\omega_p}{p}$

Given that energetic pulses from near source records can be as long as 2 s and wind turbines can be as tall as 140 m, ω_p/p for a design earthquake could be as large as 12.7. A bound of $\omega_p/p = 10$ is chosen because larger values correspond to unrealistically large overturning accelerations.

- Slenderness of the structure α

Damping because of impact is strongly influenced by slenderness: the squatter the structure is, the more energy it loses in every impact. Thus, accurate modeling of the energy dissipated at impact for structures with large α is important. Typical slenderness values for wind turbine structures were judged to be smaller than 0.2. Hence, only structures with slenderness $\alpha = 0.1$ and $\alpha = 0.2$ are studied.

- Dimensionless masses γ_{mc}, γ_{mb} and γ_{Ib}

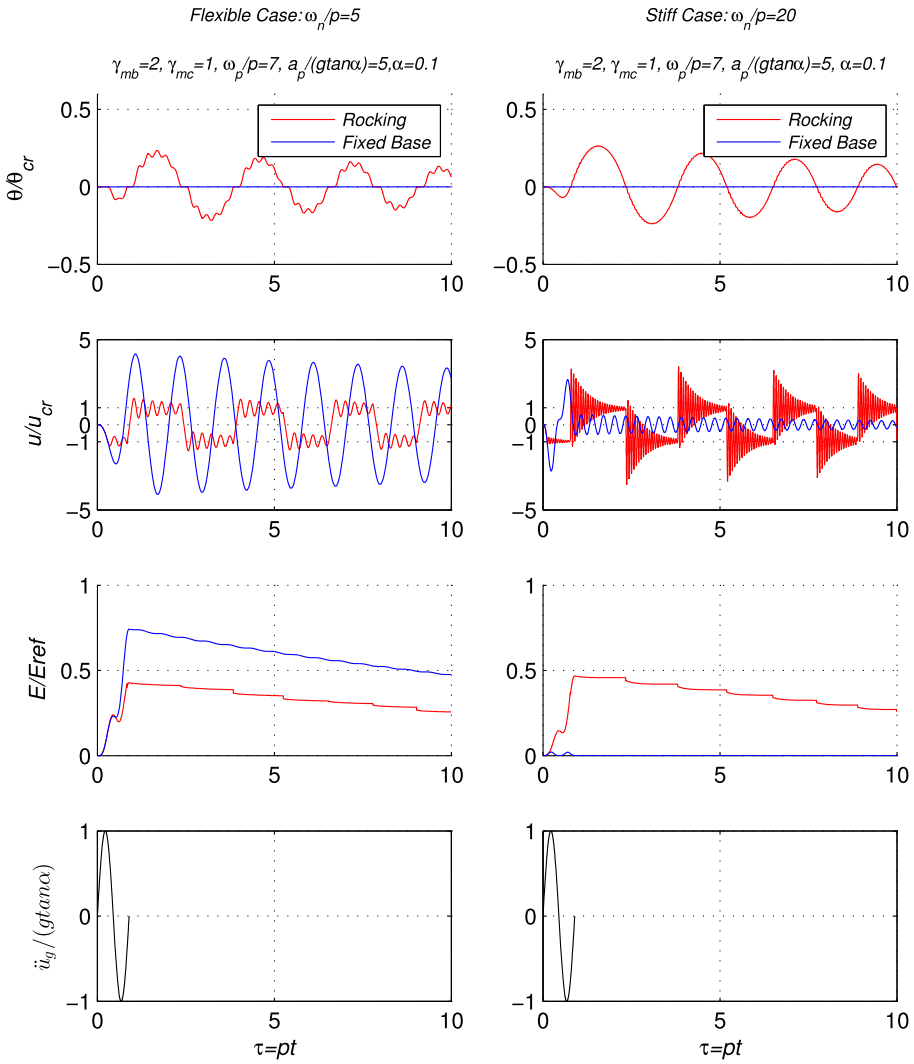

Figure 5. Comparison of the response of flexible (left) and stiff (right) deformable rocking columns.

DOI: 10.1002/eqe

Wind turbine nacelles and propellers amount a top mass of the order of 100 tons [47] making $\gamma_{mc} < 2$. The diameter of a circular mat foundation for a conventional 100 m tall on-shore wind turbine needs to be smaller than 20 m to give the structure a slenderness ratio of $\alpha < 0.2$. Conventional reinforced concrete mat foundations of this size would be 50 to 100 times heavier than the turbine tower, the generator and the propeller together. Hence, a lighter foundation, e.g. a prefabricated space truss foundation, is needed to let the structure uplift during an earthquake. To this end, a maximum value of $\gamma_{mb} = 2$ is examined. Ratio γ_{Ib} is equal to 1.0 for a rectangular foundation, to

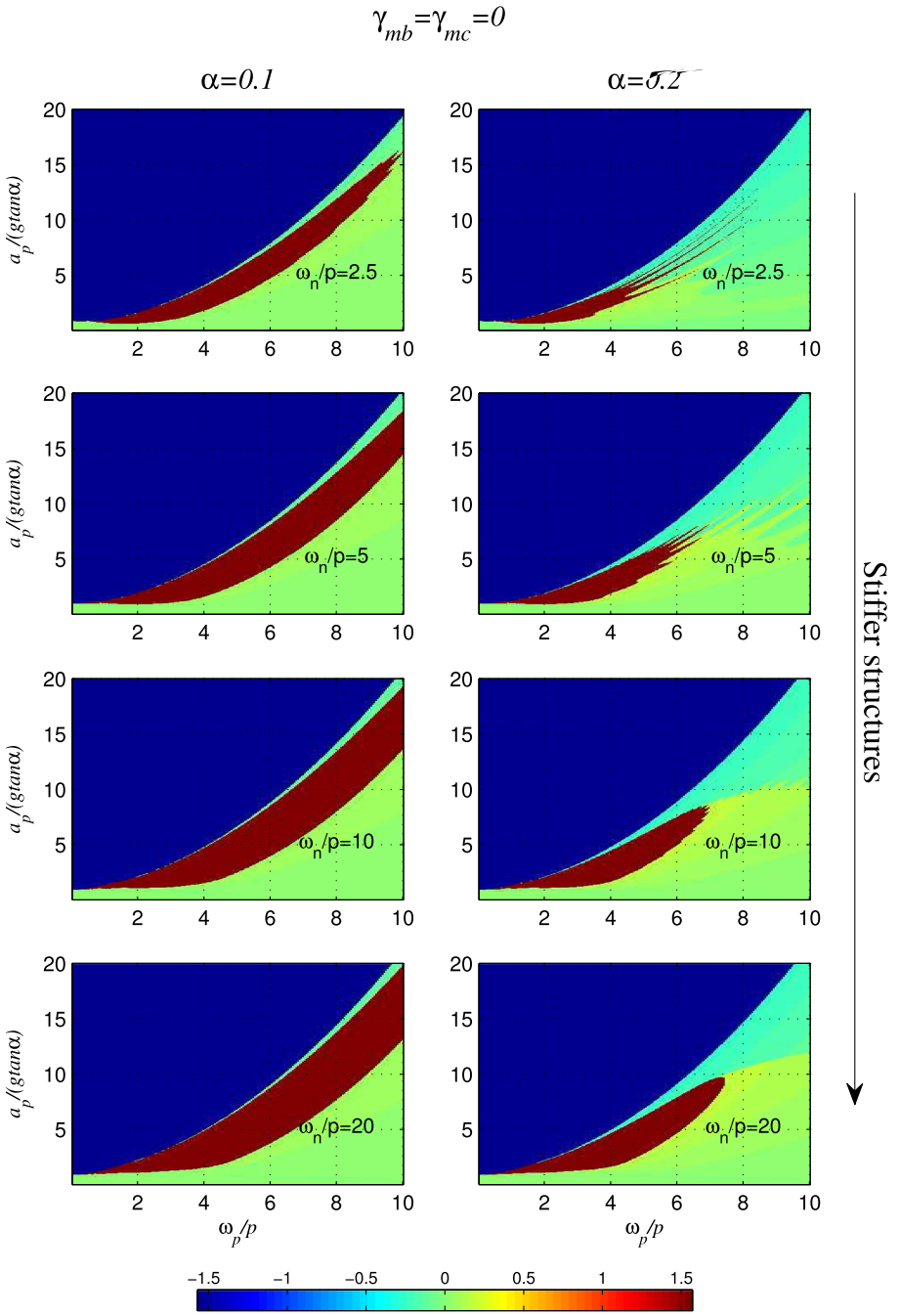

Figure 6. Rocking spectra (maximum base rotation, θ/α) of deformable rocking structures with mass only on the top for different dimensionless stiffness subjected to a one-cycle sine ground motion.

DOI: 10.1002/eqe

0.95 for a disk foundation and to 1.125 for a circular hoop foundation. Therefore, $\gamma_{Ib}=1$ for the subsequent analyses.

- Structure damping ratio: ζ

Wind turbine towers are intended to remain elastic during their response to design-basis excitation. Therefore, their fixed base structural damping is expected to be no larger than 0.01. The increase of damping in the uplifted state predicted by equation (19) was not experimentally observed [30]. Therefore, as proposed in [30], a damping ratio of 0.01/S (where S is equal to

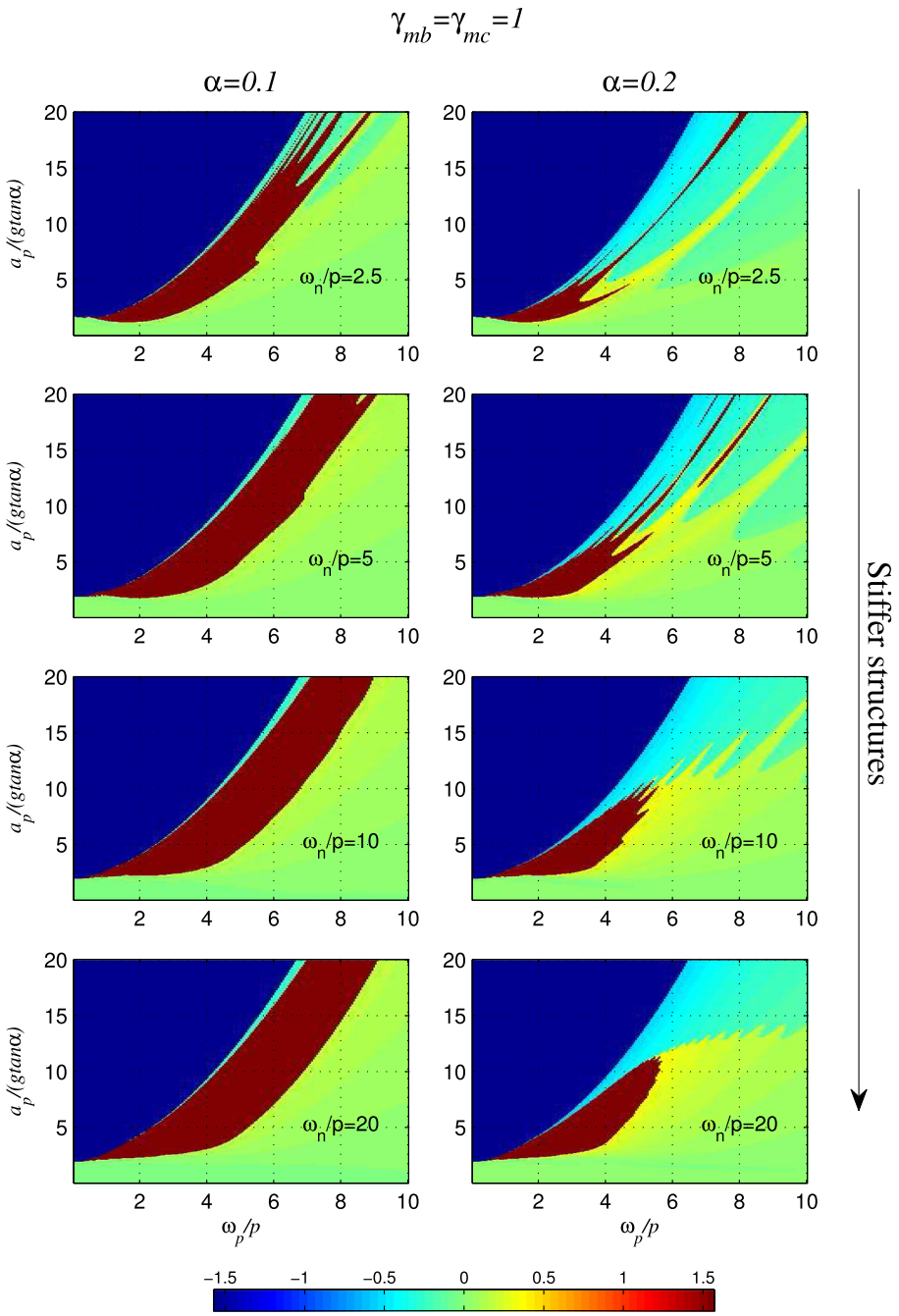

Figure 7. Rocking spectra (maximum base rotation, θ/α) of deformable rocking structures with $\gamma_{mb}=\gamma_{mc}=1$ and different dimensionless stiffness values subjected to a one-cycle sine ground motion.

DOI: 10.1002/eqe

the square root term in equation (19)) is used. This way the uplifted damping will be constant and equal to 0.01.

3.2. *General observations on the dynamic response of the deformable rocking cantilever*

The dimensionless response of two deformable (one flexible and one stiff, but not rigid) rocking cantilever column models (Figure 1) subjected to a one-cycle sinus acceleration pulse with amplitude equal to a_p and cyclic frequency equal to ω_p was computed and is plotted in Figure 5.

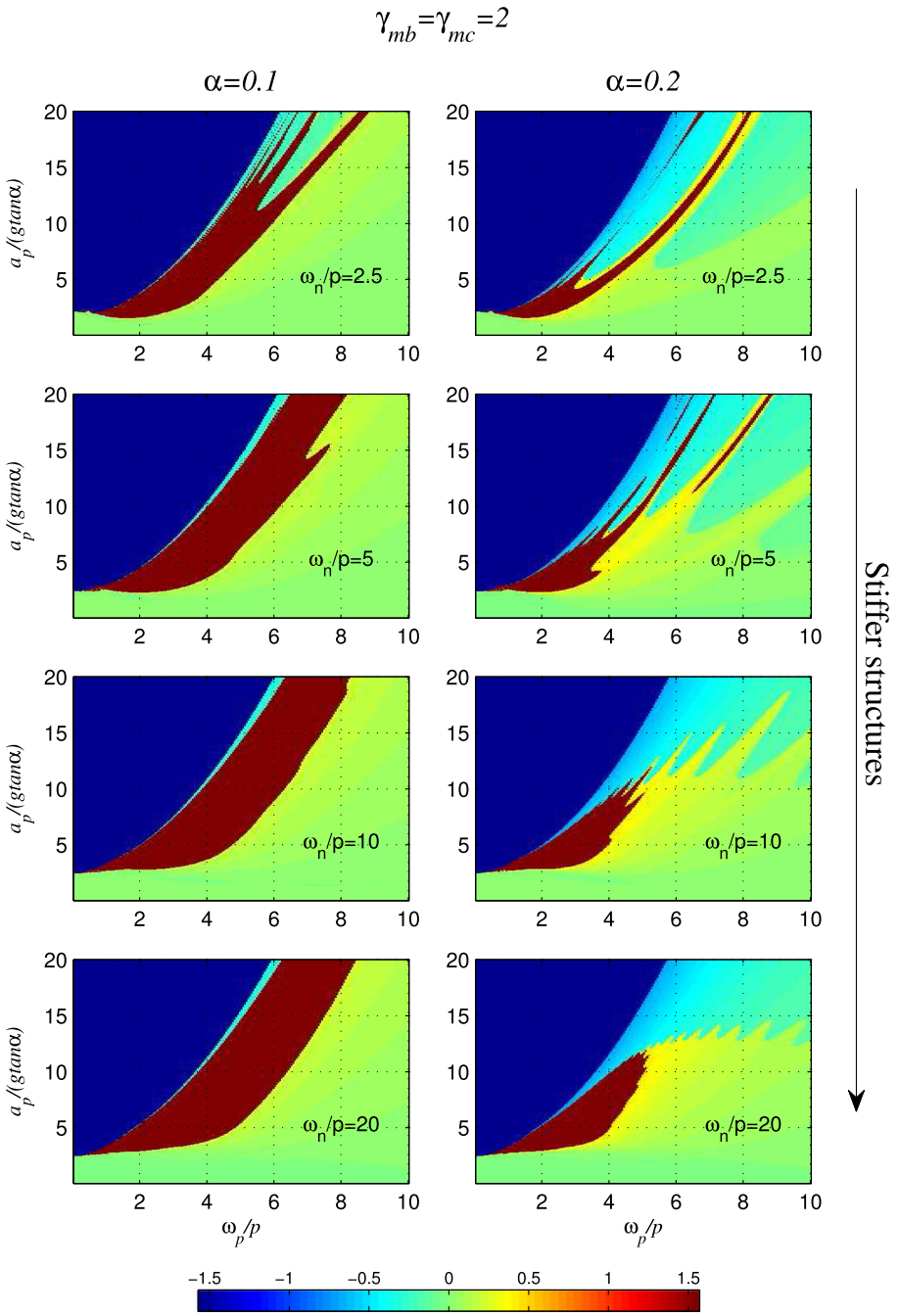

Figure 8. Rocking spectra (maximum base rotation, θ/α) of deformable rocking structures with $\gamma_{mb}=\gamma_{mc}=2$ and different dimensionless stiffness values subjected to a one-cycle sine ground motion.

DOI: 10.1002/eqe

The flexible model has $\omega_n/p = 5$ and the stiff model has $\omega_n/p = 20$. Based on equation (42) these values correspond to 123 m and 16 m tall wind turbines with fundamental vibration periods of 4.5 s and 0.4 s, respectively. The slenderness value for both wind turbines is 0.1. The structure damping ratio is $\zeta = 0.005$. The response is a superposition of a low frequency rocking motion and a high frequency elastic oscillation around a value of u slightly smaller than u_{cr}.

In the uplifted state, both models oscillate elastically with a frequency higher than that for the corresponding fixed-base case. Counting cycles gives that the flexible model oscillates with a frequency $\omega/p = 23.83$ and the stiff one with a frequency $\omega/p = 92.59$. Equation (18) gives 23.08 and 93.32, respectively. The apparent damping ratio in the uplifted state is also much larger than that of the corresponding fixed-base column.

The use of a low structure damping ratio ($\zeta = 0.005$) reveals another phenomenon, not previously observed. Because elastic oscillation amplitudes decay at a rate proportional to $\zeta_{up}\omega_{up}$, the time interval between two impacts is long enough for the elastic oscillations of the stiff model to damp out. However, this is not the case for the flexible model. Hence, the flexible model impacts while still oscillating. As it will be shown in the next section, this phenomenon affects the shape of the rocking spectra.

Another major difference between the stiff and the flexible cases is the relative amplitude (u/u_{cr}) of the elastic oscillations. As observed experimentally [40, 30, 48], stiff structures oscillate strongly after every impact. These oscillations can be so strong that, in the case shown in Figure 5 (right), they result in larger displacements of the rocking model than those of the corresponding fixed-base model.

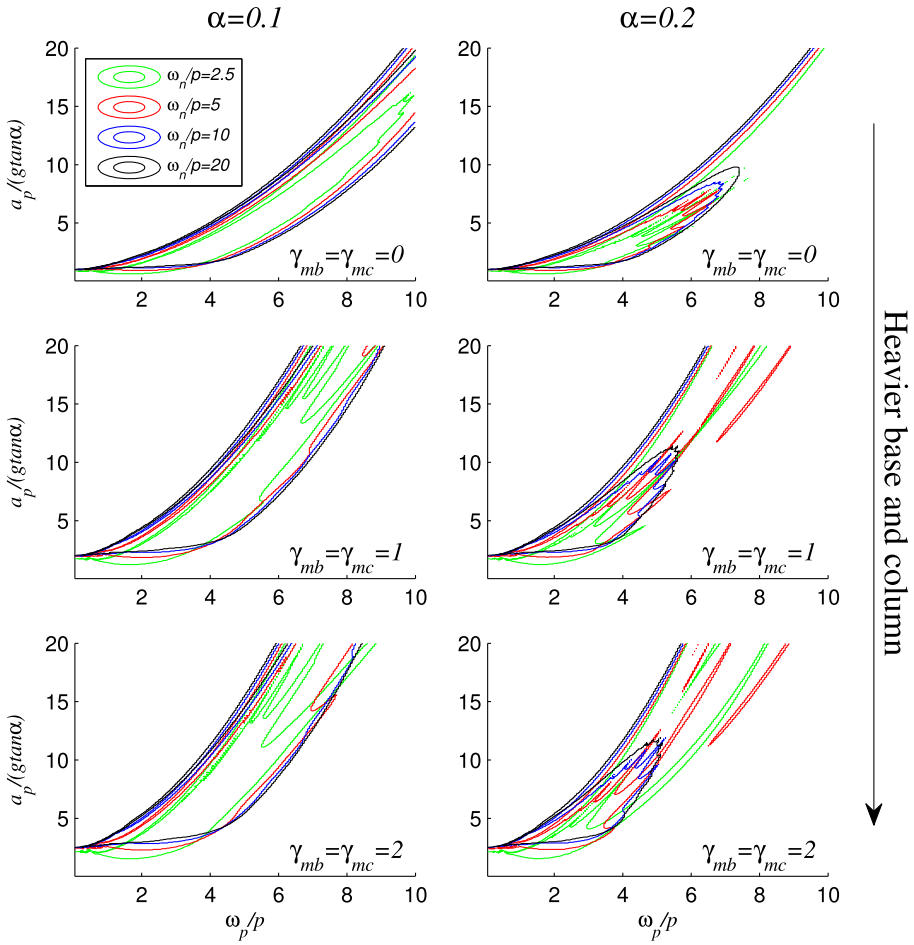

Figure 9. Overturning spectra for deformable rocking structures subjected to a one-cycle sine ground motion.

DOI: 10.1002/eqe

However, in the flexible case, the oscillations are much smaller and the maximum displacements are smaller than those of the fixed-base counterpart.

3.3. *Rocking spectra*

Figures 6–8 plot the rocking spectra (maximum rotation θ vs. ω_p/p and $a_p/g\tan\alpha$) of the deformable rocking cantilever model (Figure 1) subjected to a one-cycle sinus acceleration pulse with amplitude equal to a_p and cyclic frequency equal to ω_p. Figure 9 plots the contour plot of maximum rotation θ. The contour lines represent the border between overturning and remaining upright. The most important finding is that deformable rocking columns qualitatively retain the size effect inherent to rigid rocking columns: a very intense pulse (one with a very high acceleration) is needed to overturn a very large rocking column regardless of its deformability. In case of overturning without impact (blue area in Figures 6–8) the values of overturning acceleration are only slightly affected by deformability of the rocking column: more flexible columns need slightly lower accelerations to overturn than stiffer (and rigid) ones. However, for overturning after one impact (brown area in Figures 6–8), even though the size effect still qualitatively exists, the rocking spectra of the

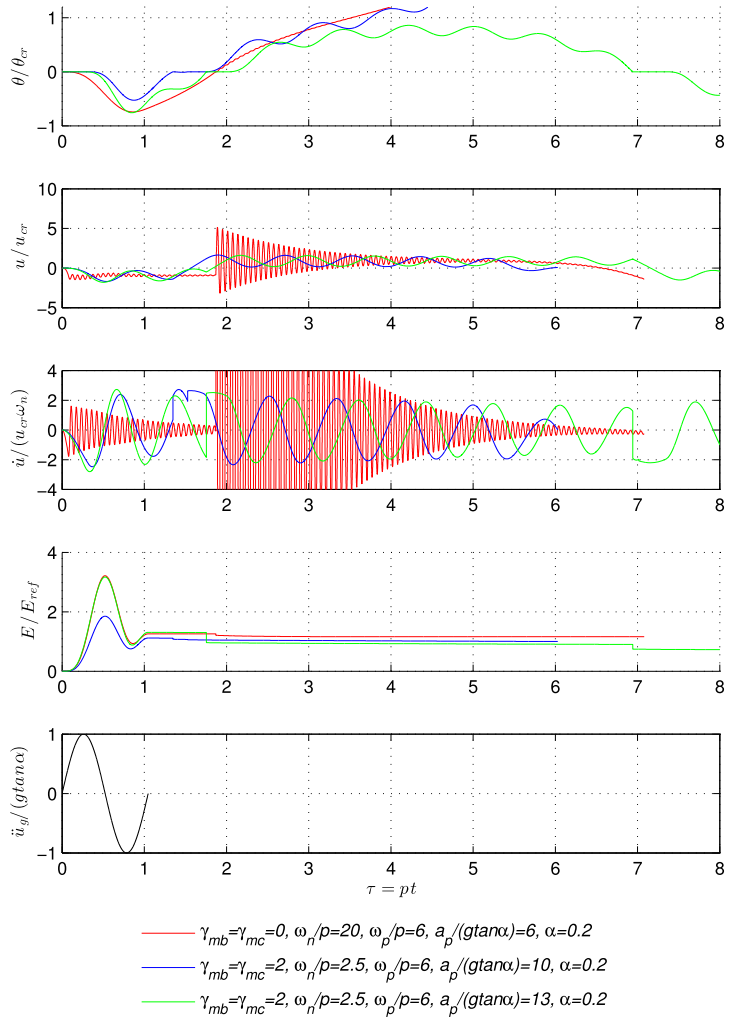

Figure 10. Rotation, elastic displacement, elastic velocity and energy time histories for a stiff (red) and two flexible (blue and green) deformable rocking cantilever structures excited by one-cycle sine ground motions (black) with different intensities.

DOI: 10.1002/eqe

deformable rocking cantilever (Figure 1) have two characteristics that are not present in the rigid column rocking spectra:

(1) For small values of ω_p/p ($\omega_p/p < 4$) the overturning-with-impact area of the rocking spectrum descends ('sinks', as pointed out by Acikgoz and DeJong [29]). This phenomenon is more pronounced as the base, i.e. γ_{mb}, becomes larger. Evidently, spectral accelerations of fixed-base columns with ω_p/p values in this range are larger than PGA. However, even for earthquakes with a pulse period as long as $T_p = 2$ s, the threshold of $\omega_p/p = 4$ corresponds to a cantilever structure with $R \approx 16$ m ($p \approx 0.79$). Based on equation (41), an $R = 16$ m wind turbine is relative stiff (dimensionless stiffness $\omega_n/p \approx 20$) resulting in small 'sinking' of the overturning-with-impact area compared to the rocking spectra of a rigid rocking cantilever.

(2) For larger values of ω_p/p ($\omega_p/p > 4$), i.e. for larger and more deformable structures and for relatively flexible smaller structures, the overturning-with-impact area for deformable rocking cantilevers ceases to have the well-known smooth shape that it has for rigid rocking structures, as well as for the flexible ones presented in [29]. This phenomenon is more pronounced: (i) for heavier bases and for smaller column stiffness (i.e. for smaller uplifted frequencies); and (ii) for more squat structures where the energy dissipation at every impact is larger, hence more important. Figure 10 illustrates this behavior. Plotted are: the response of a stiff structure with mass only on the top that overturns after one impact (hence it belongs in the smooth brown area of the bottom-right spectrum of Figure 6); and the response of a flexible structure with $\gamma_{mb} = \gamma_{mc} = 2$ (top-right spectrum of Figure 8) for different one-cycle sine pulse amplitudes. The flexible structure survives the stronger pulse ($a_p/g\tan\alpha = 15$) but is overturned by the weaker pulse ($a_p/g\tan\alpha = 14.5$). The reason for this is that the flexible structure still oscillates at the instant of impact. It so happens that in the case of the stronger pulse (green line) the prior-to-impact elastic displacements and velocities, u and $\dot{u}$ are smaller (in absolute value) than in the case of the weaker pulse (blue line). Hence, according to equations (26) and (27) the energy loss in the case of the stronger pulse is larger, as seen in the 4th plot of Figure 10. In other words, if the structure has not stopped vibrating elastically before the impact happens, then the position of its masses will depend on the deformed vibration shape at the instant of impact and will be essentially random. Thus, the value of the eccentricity of the oscillating structure is changing as it oscillates, causing the coefficient of restitution at impact to change randomly. This causes the non-smoothness of the spectra. The relation of the eccentricity of a rocking object and the coefficient of restitution is studied in [49].

4. CONCLUSIONS

A model to compute the rocking response of a deformable rocking cantilever with a distributed mass and a massive base and top (Figure 1) has been proposed. This model extends the previously developed models [25, 26, 29] and introduces a novel model for energy dissipation at impact. The proposed modified model was verified and validated by comparing the computed response to the response measured in a suite of deformable rocking column experiments described in the companion paper [30]. The proposed model was then used to construct rocking spectra for deformable rocking structures exposed to sinusoid pulse ground motion excitations. The presence of the column and base masses decreases the uplifted frequency (compared to the model with a single mass at the top) and therefore emphasizes the effect of column flexibility. However, it was shown that for large structures or relatively high frequency sinusoid pulses, the effect of flexibility is still not detrimental to the stability of the structure. Thus, large deformable cantilever structures, such as tall bridge columns, chimneys and wind turbines, uplift and rock without overturning under dynamic ground motion excitation. This remarkable property can be used to limit the design bending moments and shear forces at the base of large deformable structures, thus making them more economical to construct while keeping the risk of overturning less than or equal to the risk of collapse of the corresponding fixed base structures.

DOI: 10.1002/eqe

APPENDIX: DERIVATION OF THE EQUATIONS OF MOTION

With reference to Figure 1 and after placing the origin of the axis at the pivot point, the position vector of a point of the column is:

$$\mathbf{r} = \begin{bmatrix} -sign(\theta)B\cos\theta + \xi\sin\theta + u\psi\cos\theta \\ sign(\theta)B\sin\theta + \xi\cos\theta - u\psi\sin\theta \end{bmatrix} \tag{A1}$$

and the velocity vector of the same point is

$$\dot{\mathbf{r}} = \begin{bmatrix} sign(\theta)B\sin\theta\cdot\dot{\theta} + \xi\cos\theta\cdot\dot{\theta} + \dot{u}\psi\cos\theta - u\psi\sin\theta\cdot\dot{\theta} \\ sign(\theta)B\cos\theta\cdot\dot{\theta} - \xi\sin\theta\cdot\dot{\theta} - \dot{u}\psi\sin\theta - u\psi\cos\theta\cdot\dot{\theta} \end{bmatrix}, \tag{A2}$$

$$\|\dot{\mathbf{r}}\|^2 = \left(B^2 + \xi^2 + u^2\psi^2 - sign(\theta)2Bu\psi\right)\left(\dot{\theta}\right)^2 + \psi^2\dot{u}^2 + 2\xi\psi\dot{u}\dot{\theta}. \tag{A3}$$

The kinetic energy of the system is:

$$\begin{aligned} T = {} & \frac{1}{2}I_{bc}\dot{\theta}^2 + \frac{1}{2}m_c\left(\left(B^2 + \frac{H^2}{3} + \frac{33}{140}u^2 - sign(\theta)\frac{3}{4}Bu\right)\dot{\theta}^2 + \frac{33}{140}\dot{u}^2 + \frac{11}{20}H\dot{u}\dot{\theta}\right) + \\ & + \frac{1}{2}m\left(\left(B^2 + H^2 + u^2 - sign(\theta)2Bu\right)\dot{\theta}^2 + \dot{u}^2 + 2H\dot{u}\dot{\theta}\right). \end{aligned} \tag{A4}$$

The potential energy (from gravity, D' Alembert forces and strain energy) is:

$$\begin{aligned} V = {} & g\left(\begin{array}{l} sign(\theta)m_bB\sin\theta + m_c\left(sign(\theta)B\sin\theta + \frac{H}{2}\cos\theta - \frac{3}{8}u\sin\theta\right) + \\ +m(sign(\theta)B\sin\theta + H\cos\theta - u\sin\theta) \end{array}\right) + \\ & + \ddot{u}_g\left(\begin{array}{l} -sign(\theta)m_bB\cos\theta + m_c\left(-sign(\theta)B\cos\theta + \frac{H}{2}\sin\theta + \frac{3}{8}u\cos\theta\right) + \\ +m(-sign(\theta)B\cos\theta + H\sin\theta + u\cos\theta) \end{array}\right) + \\ & + \frac{13EI}{2H^3}u^2. \end{aligned} \tag{A6}$$

Lagrange equations:

$$\frac{d}{dt}\frac{\partial(T-V)}{\partial\dot{\theta}} - \frac{\partial(T-V)}{\partial\theta} = 0, \tag{A7}$$

$$\frac{d}{dt}\frac{\partial(T-V)}{\partial\dot{u}} - \frac{\partial(T-V)}{\partial u} = -c\dot{u} \tag{A8}$$

give equations (8) and (9).

REFERENCES

1. Milne, J. Seismic experiments. *Trans. Seism. Soc. Japan* 1885; **8**: 1–82.
2. Housner GW. The behaviour of inverted pendulum structures during earthquakes. *Bulletin of the Seismological Society of America* 1963; **53**(2): 404–417.
3. Zhang J, Makris N. Rocking response of free-standing blocks under cycloidal pulses. *Journal of Engineering Mechanics, ASCE* 2001; **127**(5): 473–483.

DOI: 10.1002/eqe

4. Makris N, Konstantinidis D. The rocking spectrum and the limitations of practical design methodologies. *Earthquake Engineering and Structural Dynamics* 2003; **32**: 265–289.
5. Makris N, Vassiliou MF. Planar rocking response and stability analysis of an array of free standing columns capped with a freely supported rigid beam (2012). *Earthquake Engineering and Structural Dynamics* 2013; **42**(3): 431–449.
6. Makris N, Vassiliou MF. Are some top-heavy structures more stable?. *Journal of Structural Engineering* 2014; **140**(5): 06014001.
7. Apostolou M, Gazetas G, Garini E. Seismic response of slender rigid structures with foundation uplifting, *Soil Dynamics and Earthquake Engineering* 2007; **27**(7): 642–654
8. Gelagoti F, Kourkoulis R, Anastasopoulos I, Gazetas G. Rocking isolation of low-rise frame structures founded on isolated footings. *Earthquake Engineering and Structural Dynamics* 2012; **41**: 1177–1197.
9. Antonellis G, Panagiotou M. Seismic response of bridges with rocking foundations compared to fixed-base bridges at a near-fault site. *Journal of Bridge Engineering* 2013; **19**(5): 04014007.
10. Makris N. The role of the rotational inertia on the seismic resistance of free-standing rocking columns and articulated frames. *Bulletin of the Seismological Society of America* 2014; **104**(5): 2226–2239.
11. Makris N. A half-century of rocking isolation. *Earthquakes and Structures* 2015; **7**(2): 1187–1221.
12. Ricles JM, Sause R, Garlock MM, Zhao C. Posttensioned seismic-resistant connections for steel frames. *Journal of Structural Engineering* 2001; **127**(2): 113–121.
13. Priestley MN, Sritharan S, Conley JR, Pampanin S. Preliminary results and conclusions from the PRESSS five-story precast concrete test building. *PCI Journal* 1999; **44**(6): 42–67.
14. Pampanin S, Priestley MN, Sritharan S. Analytical modelling of the seismic behaviour of precast concrete frames designed with ductile connections. *Journal of Earthquake Engineering* 2001; **5**(03): 329–367.
15. Christopoulos C, Filiatrault A, Uang CM, Folz B. Posttensioned energy dissipating connections for moment-resisting steel frames. *Journal of Structural Engineering* 2002; **128**(9): 1111–1120.
16. Christopoulos C, Filiatrault A, Folz B. Seismic response of self-centring hysteretic SDOF systems. *Earthquake Engineering and Structural Dynamics* 2002; **31**(5): 1131–1150.
17. Eatherton MR, Ma X, Krawinkler H, Mar D, Billington S, Hajjar JF, Deierlein GG. Design concepts for self-centering rocking steel braced frames. *Journal of Structural Engineering, American Society of Civil Engineers* 2014; **140**(11): 04014082.
18. Eatherton MR, Ma X, Krawinkler H, Deierlein GG, Hajjar JF. Quasi-static cyclic behavior of controlled rocking steel frames. *Journal of Structural Engineering, American Society of Civil Engineers* 2014; **140**(11): 04014083.
19. Makris N, Vassiliou M. Dynamics of the rocking frame with vertical restrainers. *Journal of Structural Engineering* 2014; DOI: 10.1061/(ASCE)ST.1943-541X.0001231
20. Beck JL, Skinner RI. The seismic response of a reinforced concrete bridge pier designed to step. *Earthquake Engineering and Structural Dynamics* 1973; **2**: 343–358.
21. Ma, QT, Khan, MH. Free vibration tests of a scale model of the South Rangitikei Railway Bridge. In *Proceedings of the New Zealand Society for Earthquake Engineering Annual Conference*, *Engineering an Earthquake Resilient NZ.* 2008.
22. Sharpe RD, Skinner RI, The seismic design of an industrial chimney with rocking base. *Bulletin of the New Zealand National Society for Earthquake Engineering* 1983; **16**(2): 98–106
23. Papadopoulos C. DOMOS Engineers, Athens, Greece, personal communication, September 19, 2014
24. Psycharis IN, Jennings PC. Rocking of slender rigid bodies allowed to uplift. *Earthquake Engineering and Structural Dynamics* 1983; **11**: 57–76.
25. Oliveto G, Caliò I, Greco A. Large displacement behaviour of a structural model with foundation uplift under impulsive and earthquake excitations. *Earthquake Engineering and Structural Dynamics* 2003; **32**: 369–393.
26. Ma QTM. The mechanics of rocking structures subjected to ground motion (Doctoral dissertation, ResearchSpace@ Auckland). 2010
27. Chopra AK, Yim SCS. Simplified earthquake analysis of structures with foundation uplift. *Journal of Structural Engineering* 1985; **111**(4): 906–930.
28. Vassiliou MF, Mackie KR, Stojadinović B. Dynamic response analysis of solitary flexible rocking bodies: modeling and behavior under pulse-like ground excitation. *Earthquake Engineering and Structural Dynamics* 2014; **43**: 1463–1481
29. Acikgoz S, DeJong MJ. The interaction of elasticity and rocking in flexible structures allowed to uplift. *Earthquake Engineering and Structural Dynamics* 2012; **41**(15): 2177–2194.
30. Truniger R, Vassiliou MF, Stojadinovic B. An analytical model to study deformable cantilever structures rocking on a rigid surface: experimental verification, *Earthquake Engineering and Structural Dynamics* 2015. (submitted for possible publication)
31. Vassiliou MF, Makris N. Analysis of the rocking response of rigid blocks standing free on a seismically isolated base. *Earthquake Engineering and Structural Dynamics* 2012; **41**(2): 177–196.
32. Chopra AK. *Dynamics of Structures* (Vol. **3**). Prentice Hall: New Jersey, 1995
33. Peña F, Prieto F, Lourenço PB, Campos Costa A, Lemos JV. On the dynamics of rocking motion of single rigid-block structures. *Earthquake Engineering and Structural Dynamics* 2007; **36**(15): 2383–2399.
34. ElGawady MA, Ma Q, Butterworth JW, Ingham J. Effects of interface material on the performance of free rocking blocks. *Earthquake Engineering and Structural Dynamics* 2011; **40**(4): 375–392.
35. Hogan SJ. The many steady state responses of a rigid block under harmonic forcing. *Earthquake Engineering and Structural Dynamics* 1990; **19**(7): 1057–1071.

DOI: 10.1002/eqe

36. Dimitrakopoulos EG, DeJong MJ. Revisiting the rocking block: closed-form solutions and similarity laws. *Proceedings of the Royal Society A: Mathematical, Physical and Engineering Science* 2012; **468**(2144): 2294–2318.
37. Prieto F, Lourenço PB, Oliveira CS. Impulsive Dirac-delta forces in the rocking motion. *Earthquake Engineering and Structural Dynamics* 2004; **33**(7): 839–857.
38. Zhang H, Brogliato B, Liu C. Dynamics of planar rocking-blocks with Coulomb friction and unilateral constraints: comparisons between experimental and numerical data. *Multibody System Dynamics* 2013; **32**(1): 1–25.
39. Psycharis IN. Effect of base uplift on dynamic response of SDOF structures. *Journal of Structural Engineering* 1991; **117**(3): 733–754.
40. Acikgoz S, DeJong MJ. Analytical and experimental observations on vibration modes of flexible rocking structures, *SECED—Society for Earthquake and Civil Engineering Dynamics Young Engineers Conference*, July 4th, 2013.
41. Makris N. Rigidity–plasticity–viscosity: can electrorheological dampers protect base-isolated structures from near-source ground motions? *Earthquake Engineering and Structural Dynamics* 1997; **26**: 571–591.
42. Makris N, Chang S-P. Effect of viscous, viscoplastic and friction damping on the response of seismic isolated structures. *Earthquake Engineering and Structural Dynamics* 2000; **29**(1):85–107.
43. Vassiliou MF, Makris N. Estimating time scales and length scales in pulselike earthquake acceleration records with wavelet analysis. *Bulletin of the Seismological Society of America* 2011; **101**(2): 596–618.
44. Barenblatt GI. *Scaling, Self-Similarity, and Intermediate Asymptotics*, Cambridge University Press: Cambridge, U.K, 1996.
45. Prowell I, Veers P. Assessment of wind turbine seismic risk: Existing literature and simple study of tower moment demand. Rep. No. SAND2009-1100, Sandia National Laboratories. 2009.
46. Patrick S. (7 March 2014) Vestas creates 140-metre tower [Web log post]. Retrieved September 19, 2014, from http://www.windpowermonthly.com/
47. Hau E, Von Renouard H. *Wind Turbines: Fundamentals, Technologies, Application, Economics*. Springer: 2013.
48. Truniger R. Experimental investigation of the response of flexible rocking oscillators to ground shaking, *Master Thesis– Spring Semester 2014, ETH Zürich – Institute of Structural Engineering*, Zürich, 2014.
49. Contento A, Di Egidio A. Investigations into the benefits of base isolation for non-symmetric rigid blocks. *Earthquake Engineering and Structural Dynamics* 2009; **38**(7): 849–866.

DOI: 10.1002/eqe